sciendo

POLISH MARITIME RESEARCH Special Issue 2018 S3 (99) 2018 Vol. 25; pp. 43-53
10.2478/pomr-2018-0111

STUDY OF THE FORCE AND DEFORMATION CHARACTERISTICS OF SUBSEA MUDMAT-PILE HYBRID FOUNDATIONS

Desen Kong [1,2]
Meixu Deng[1,2]
Yi Liu[1,2]
Xiaoyan Tan[3]
[1] College of Civil Engineering and Architecture, Shandong University of Science and Technology, China
[2] Shandong Provincial Key Laboratory of Civil Engineering Disaster Prevention and Mitigation, Shandong University of Science and Technology, China
[3] Shandong Xingke Intelligent Technology Co., Ltd., China

ABSTRACT

To study the force and deformation characteristics of subsea mudmat-pile hybrid foundations under different combined loads, a project at a water depth of 200 m in the South China Sea was studied. A numerical model of a subsea mudmat-pile hybrid foundation is developed using the numerical simulation software FLAC3D. The settlement of the seabed soil, the bending moments of the mudmat, and the displacements and bending moments along the pile shaft *under different load combinations, including vertical load and horizontal load, vertical load and bending moment, and horizontal load and bending moment load, are analyzed. The results indicate that settlement of the seabed soil is reduced by the presence of piles. The settlement* of the *mudmat is reduced by the presence of piles. Different degrees of inclination occur along the pile shaft. The angle of inclination of pile No. 1 is greater than that of pile No. 2. The dip directions of piles No. 1 and No. 2 are identical under the vertical load and bending moment and are opposite to those under the other combined loads. The piles that are located at the junctions between the mudmat and the tops of the piles are easily destroyed.*

Keywords: Subsea Mudmat-pile Hybrid Foundations, force characteristics, deformation characteristics, combined loads

INTRODUCTION

In recent years, traditional fossil energy sources have been increasingly exhausted, and the environment has been deteriorating. Marine resources have made significant progress as a renewable energy source, and the technology for developing marine resources has matured [1-2]. Deepwater resources have been discovered, and offshore oil and gas engineering equipment has progressed from the shallow sea to the deep ocean. The deep ocean has gradually become the main area for the development of global marine resources [3-4]. As a common component in the development of deepwater oil and gas resources, subsea anti-sinking plate foundations are used as the supporting structures for wellheads, pipe sink nodes, umbilical cord cables and other components of underwater production systems. These foundations bear the load of each block of the underwater production system and transfer it to the foundation. They form the foundation of each block in the underwater production system, and they are rarely subjected to a single load during operations [5-8]. Due to the complex environmental conditions of the seabed, these foundations are usually subjected to two or more loads simultaneously. Because of the limitations of the anti-horizontal load and anti-overturning capabilities of anti-sinking plates, their bearing capacity is low. To overcome the limitations in the application of anti-sinking plates, piles

are added under them to form composite foundations, which bear part of the horizontal load and overturning bending moment to reduce the size of the anti-sinking plate.

Foreign scholars have conducted numerous studies on anti-sinking panels, and several results have been achieved. Yun simplified the seabed as a homogeneous soil and analyzed the bearing capacity envelope lines of three types of anti-sinking plate foundations in the V-H-T load space using a numerical method [9]. Bransby studied the bearing characteristics of a skirt plate of an anti-sinking plate foundation in the V-H-M composite load space by means of numerical calculations [10-11]. However, few domestic studies have focused on subsea anti-sinking plates; in particular, mudmat-pile hybrid foundations have rarely been studied. Based on practical engineering, provide examples of using industry standards to design anti-sinking plate foundations [12-14].

Using the FLAC3D finite difference software, numerical models of subsea mudmat-pile hybrid foundations can be eveloped to study their force and deformation characteristics under different load combinations. By applying combined loads to the model, such as a vertical load and a horizontal load, a vertical load and a bending moment, and a horizontal load and a bending moment, analyses of the seabed soil settlement, the bending moments of the anti-sinking plate, and the displacements and bending moments along the pile shaft can be performed, which have theoretical significance.

DEVELOPMENT OF THE NUMERICAL MODEL

Taking a 200 m water depth project in the South China Sea as an example, a separation-type mudmat-pile hybrid foundation is simplified as an anti-sinking plate and angle piles. A numerical simulation model of the subsea mudmat-pile is developed using the FLAC3D numerical simulation software, which is also used to determine the constitutive model of the seabed soil, the unit types of the anti-sinking plate model and the pile model, and their various physical and mechanical parameters.

The FLAC3D finite difference equation is as follows:

$$\int_S n_i f \mathrm{d}s = \int_A \frac{\partial f}{\partial x_i} \mathrm{d}A \tag{1}$$

In Eq (1):
$\int_S$ – The integral around the boundary of the closed surface;
n_i – The unit normal vector of s;
f – A scalar, vector, or tensor;
x_i – The coordinate vector; $\mathrm{d}s$ is the incremental arc length;
$\int_A$ – The integral of the surface area A.

CONSTRUCTION OF THE SOIL BODY MODEL

The soil body model is built as a six-sided block body with a built-in grid. The model is 50 m long, 25 m wide and 20 m deep. The lower left corner of the model is taken as the coordinate origin. Considering the accuracy of the numerical calculations and the size requirements of the grid, the elements of the soil body model are all constructed with 1 m×1 m×1 m positive-cube cells, and the entire model includes 25,000 zones and 27,846 grid points. The three-dimensional numerical calculation model is shown in Fig. 1.

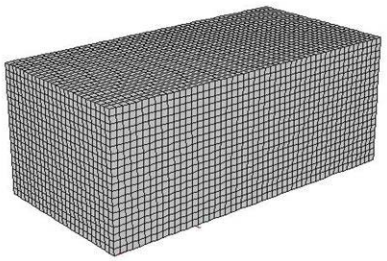

Fig. 1. Model of the seabed soil

Based on the actual conditions of the South China Sea, the seabed soil body is modeled as saturated soft clay. To utilize few parameters and simplify the measurements, the Mohr-Coulomb model is adopted for the seabed soil body model, and the material parameters are listed in Tab. 1. In the model, the boundary parallel to the x axis limits the velocity in the x direction, the boundary parallel to the y axis limits the velocity in the y direction, the bottom boundary limits the velocity in the z direction, and the top boundary is free.

Tab. 1. Material parameters of the seabed soil

bulk modulus /Pa	shear modulus /Pa	cohesion /Pa	internal friction angle /(°)	saturatd density /kg·m^{-3}
4.2×10^7	1.83×10^7	12×10^3	23	2000

DEVELOPMENT OF THE MODEL OF THE MUDMAT-PILE STRUCTURE SYSTEM

In the numerical model, structural units were used to build the mudmat-pile structure model, lining structures were used to build the anti-sinking plate model, pile structures were used to build the pile models, and point to point connections were established between the anti-sinking plate and the piles. The model, size of the anti-sinking plate and pile layout are shown in Fig. 2

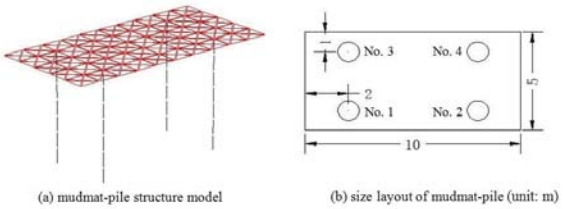

Fig. 2. Model of the mudmat-pile structure

The lining structural unit is shown in Fig. 3. It consists of a flat shell unit with three joints and can resist surface loads and bending loads. Thin plate theory is adopted in the analysis, and the deformation caused by transverse shear is ignored. The mechanical properties of the lining unit can be divided into the response of the lining material itself to the structure and the interaction between the lining and the mesh. The lining unit can consider tangential friction and normal compressive (tensile) action with the rock and soil body, and it can be detached (or embedded) from the rock and soil body. The lining structure unit is mainly used to simulate the structure with normal and tangential forces on the rock and soil body, which can withstand tension in the normal direction and simulate separation between the anti-sinking plate and the seabed soil body. Frictional slip between the anti-sinking plate and the seabed soil in the tangential direction can be simulated [15].

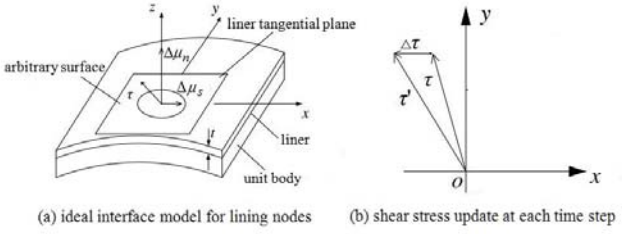

Fig. 3. Diagram of the liner structural element

The apparent stiffness of the unit in the normal direction to the lining surface is:

$$\max\left[\frac{\left(K+\frac{4}{3}G\right)}{\Delta Z_{\min}}\right] \tag{2}$$

In Eq (2):

K and G – The volume modulus and bulk modulus, respectively;

$\Delta Z_{\min}$ – The minimum size of the adjacent unit normal to the lining.

As shown in Fig. 4, the pile unit is a two-node slender unit with 6 degrees of freedom at each node and anti-bending and axial anti-tensile (anti-pressure) characteristics. It is composed of a combination of a beam element and a bar element. The interaction between the pile element and the soil grid is realized by nonlinear, sliding tangential and normal coupling springs. The tangential spring can simulate the tangential action of the grouting anchor rod, the normal spring can simulate the extrusion between the pile and the soil, and the force and displacement can be transmitted between the pile and the foundation soil by unit nodes.

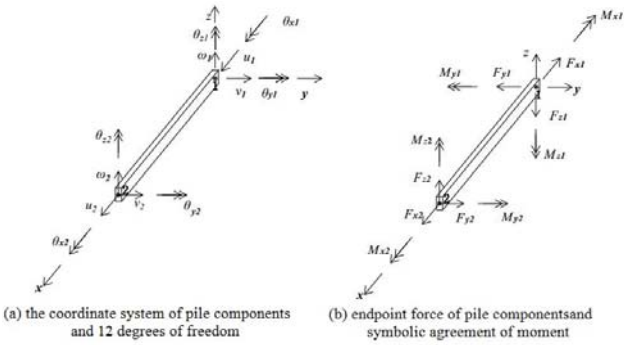

Fig. 4. Diagram of the pile element

The shear characteristics of the model pile and the mesh contact surface are mainly its natural cohesive force and friction force. The characteristics of the tangential coupling spring include the stiffness k_s, cohesion C_s, internal friction angle ϕ_s, and radius of the pile's external boundary. As shown in Fig. 5, the action of the tangential spring around the pile body is reflected by these parameters and the effective stress around the pile body.

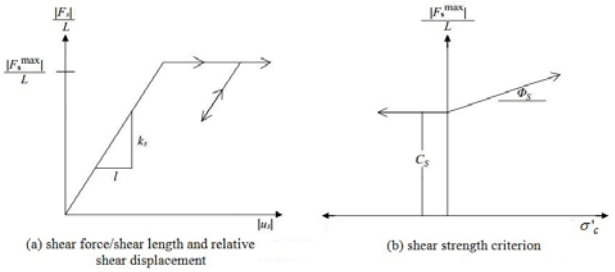

Fig. 5. Shear material behavior of piles

The shear force of a unit length pile [16] is:

$$\frac{F_s}{L} = k_s\left(u_p - u_m\right) \tag{3}$$

In Eq (3):

k_s – The shear stiffness of the connecting spring;

u_p – The axial displacement of the pile;

u_m – The axial displacement at the interface between the rock and soil.

The maximum shear force per unit length is:

$$\frac{F_{s\max}}{L} = c_s + \sigma'_c \times \tan\phi_s \times l \tag{4}$$

In Eq (4):

c_s – The bonding strength of the shear coupling spring;

σ'_c – The average effective lateral stress perpendicular to the pile unit;

ϕ_s – The friction angle of the shear coupling spring;

l – The exposed perimeter of the unit.

The average effective lateral limit stress perpendicular to the unit is:

$$\sigma'_c = -\left(\frac{\sigma_n + \sigma_m}{2} + p\right) \quad (5)$$

In Eq (5):

$\sigma_n = \sigma_x v_1^2 + \sigma_y v_2^2 + 2\sigma_{xy} v_1 v_2$;
v_i – is the unit vector;
σ_m – is the stress outside the plane;
p – is the pore pressure.

As shown in Fig. 6, the characteristic parameters of the normal coupled spring include the stiffness k_n, cohesion C_n, internal friction angle ϕ_n, gap and effective stress. These parameters reflect the normal mechanical action of the pile-soil interface when the pile and soil move in the normal direction. When piles are subjected to horizontal loads, cracks will form between the pile and soil [17]. If the reverse load is applied, the gap must close first before the soil can withstand the force in the opposite direction. If the gap parameter is set to be on, the influence of the gap on the lateral load pile can be considered.

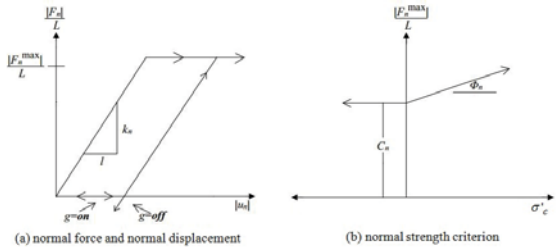

Fig. 6. Normal-direction material behavior of piles

In the model, the anti-sinking plate is 10 m long, 5 m wide and 0.2 m thick. It is simulated by lining structural units, is located in the middle of the soil body model and is in contact with its upper surface. The piles are 4 m long and 0.6 m in diameter [18]. They are simulated by pile units and are located at the four corners of the anti-sinking plate. Each pile foundation consists of 7 pile members. The top nodes of the pile and the mudmat are set as point-to-point connections. The bottom node limits the translational freedom in the three directions, and the pile has rotational freedom [19]. The mudmat-pile model includes 228 structural elements and 48 points, and the structural elements are listed in Tab. 2.

Tab. 2. Parameters of the structural elements

name	pile	mudmat
elastic modulus/GPa	206	206
Poisson's ratio	0.3	0.3
density/kg·m^{-3}	7850	7850
tangential coupling spring stiffness/GPa	13.9	0.8
normal coupling spring stiffness/GPa	1.39	0.8
tangential coupling spring bond strength/kPa	67.4	4000
normal coupling spring bond strength/kPa	67.4	—
tangential coupling spring friction angle/(°)	17.6	20
normal coupling spring friction angle/(°)	0	—

ANALYSIS OF THE NUMERICAL CALCULATION RESULTS

Using the FLAC3D numerical simulation software, a rectangular anti-sinking plate foundation is used to investigate the force and deformation characteristics of the seabed soil, the anti-sinking plate and the pile under three load combinations (vertical load and horizontal load, vertical load and bending moment, and horizontal load and bending moment load). The load conditions are listed in Tab. 3.

Tab. 3. Load conditions of mudmat-piles hybrid foundations

load name	structure self-weight/kN	vertical load/kN	horizontal load/kN	bending moment M_x/kN·m	bending moment M_y/kN·m
numerical value	470	175	345	201	305

CHARACTERISTIC ANALYSIS OF THE COMPOSITE FOUNDATION UNDER A VERTICAL LOAD AND HORIZONTAL LOAD

SETTLEMENT ANALYSIS OF THE SEABED SOIL

The settlement characteristics of the seabed soil are shown in Fig. 7. The normal surface is the section at the corner pile, and the amount of settlement of the soil decreases radially with distance from the anti-sinking plate. The maximum settlement of the soil body is 0.772 mm, and it occurs in the middle of the bottom of the anti-sinking plate [20]. The maximum positive vertical displacement of the soil body is 0.0235 mm, and it occurs at the edge of the long side of the model of the seabed soil body, which indicates that the soil far from the anti-sinking plate is slightly uplifted. As a result of the action of the angular piles, the settlement of the soil body near the piles is significantly less than that far from the piles at the same depth [21]. With increasing distance from the angular piles, their effect decreases gradually, and the settlement of the soil body caused by the piles essentially disappears at a depth of approximately 7 m. The results show that the angular pile influences the settlement of the seabed soil in a region approximately twice the length of the piles.

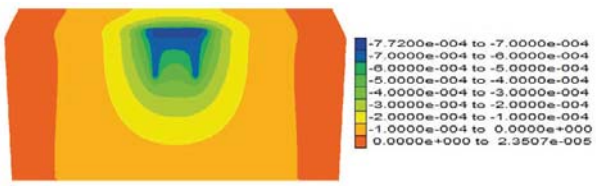

Fig. 7. Settlement of the seabed soil (units: m)

ANALYSIS OF THE BENDING MOMENTS OF THE ANTI-SINKING PLATE

The bending moment of the anti-sinking plate is shown in Fig. 8. The bending moment diagram of the anti-sinking plate is also symmetric about the *y* axis because of the structural symmetry and because the load is applied on the *y* axis. Due to the simple structure and load, the bending moment diagram of the anti-sinking plate has a clear pattern.

As shown in Fig. 8(a), the maximum positive bending moment of the anti-sinking plate in the *x* direction is 4.437 kN·m, and it is located in the middle of the long edge of the anti-sinking plate and has a semicircular distribution. The maximum negative bending moment is 19.401 kN·m and is located at the positions of the corner piles. The maximum bending moment occurs at the locations of the corner piles, which indicates that it is easy to cause damage at these locations; that is, damage to the anti-sinking plate can easily occur at the junctions between the piles and the anti-sinking plate [22]. As shown in Fig. 8(b), the maximum positive bending moment of the anti-sinking plate in the *y* direction is 1.151 kN·m, and it is located on the long edge of the anti-sinking plate and has an elongated distribution. The maximum negative bending moment is 15.376 kN·m, and it occurs at the positions of piles No. 1 and No. 2. The maximum bending moment of the anti-sinking plate is a negative bending moment that occurs at the junctions between piles No. 1 and No. 2 and the anti-sinking plate. The bending moments at piles No. 3 and No. 4 are negative and are much greater than the maximum positive bending moment, which indicates that damage to the anti-sinking plate can easily occur at the junctions between the anti-sinking plate and the piles; this is consistent with the pattern in the *x* direction bending moment diagram.

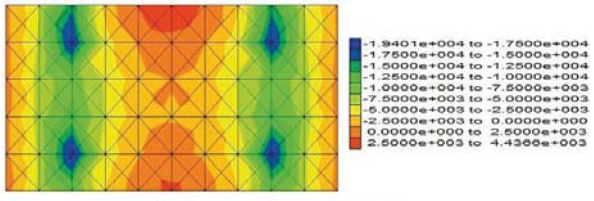

(a) bending moment diagram of mudmat M_x

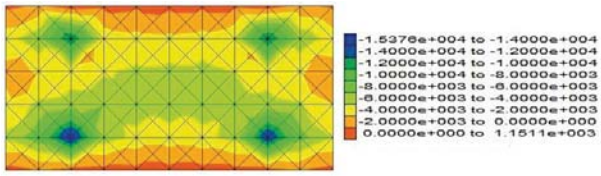

(b) bending moment diagram of mudmat M_y

Fig. 8. Bending moments of the mudmat (unit: N·m)

ANALYSIS OF THE DISPLACEMENTS ALONG THE PILE SHAFTS

Four piles are set up in the mudmat-pile hybrid foundation model, which are symmetrical to the *xoz* surface and the *yoz* plane. Piles No. 1 and No. 2 are investigated. Eight displacement monitoring positions were set from the tops of the piles to the bottoms, and 7 shear force, axial force and bending moment monitoring positions were analyzed.

The horizontal displacements of piles No. 1 and No. 2 are shown in Fig. 9. Under the combined action of the vertical and horizontal loads, pile No. 1 moves negatively along the *x* axis, and pile No. 2 moves forward along the *x* axis. The top of pile No. 1 moves 0.61×10^{-6}m in the positive direction along the *x* axis, and the bottom moves 13.11×10^{-6}m in the negative direction. The top of pile No. 2 moves 1.07×10^{-6}m in the negative direction along the *x* axis, and the bottom moves 9.914×10^{-6}m in the positive direction. The maximum displacement of pile No. 1 is 19.03×10^{-6} m, and that of pile No. 2 is 16.15×10^{-6} m, both of which occur in the middle of the piles. This may be because the pile is held fixed by the anti-sinking plate and the soil at the bottom of the pile, and the soil pressure between the corner piles under the anti-sinking plate is greater than that outside the corner piles. The horizontal displacement lines of piles No. 1 and No. 2 are smooth curves, which indicates that the pile bodies buckle. Piles No. 1 and No. 2 move in the negative horizontal direction. Pile No. 1 leans in the negative direction along the *x* axis, and pile No. 2 leans in the positive direction. The differences in displacement between the tops and bottoms of the piles are 12.5×10^{-6}m and 8.841×10^{-6} m, respectively, and the inclination angle of pile No. 1 is greater than that of pile No. 2.

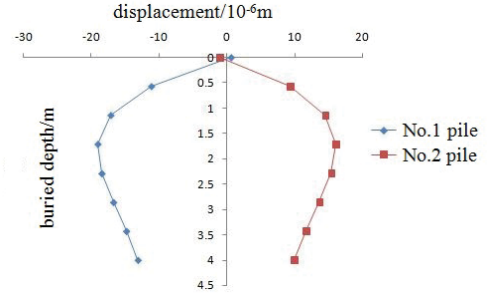

Fig. 9. Horizontal displacements along the pile shafts

The vertical displacements of piles No. 1 and No. 2 are shown in Fig. 10. The pile foundations move downward as a whole due to the combined action of the vertical and horizontal loads. The vertical displacement of the top of pile No. 2 is greater than that of pile No. 1, which indicates that the composite foundation is inclined. The vertical displacement at the top of pile No. 1 is 0.6758×10^{-3} m, and that at the bottom is 0.6768×10^{-3} m. The vertical displacement at the top of pile No. 2 is 0.6872×10^{-3} m, and that at the bottom is 0.6881×10^{-3} m. The vertical displacements of the pile bodies are greater in the middle of the piles, which is mainly caused by the stress on the bottom of the piles caused by the soil, which generates axial compression on the piles.

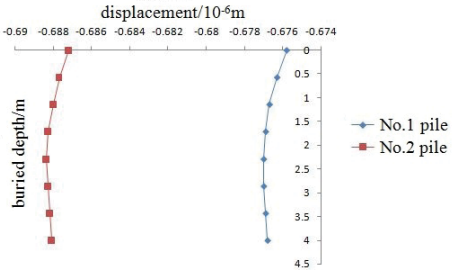

Fig. 10. Vertical displacements along the pile shafts

ANALYSIS OF THE BENDING MOMENTS ALONG THE PILE SHAFTS

The bending moments along the bodies of piles No. 1 and No. 2 are shown in Fig. 11 and Fig. 12. The bending moments of the pile bodies in the *x* direction are 0, so they are not analyzed. Due to the symmetry of the structure and the applied load, the bending moments of the two piles in the *y* direction are symmetric, and the bending moments in the *z* direction vary little.

The bending moments of the pile bodies in the *y* direction are shown in Fig. 11. Pile No. 1 has a negative bending moment of 19.58 kN·m at the junction between the pile top and the anti-sinking plate, and the bottom of pile No. 1 has a positive bending moment of 0.232 kN·m. Pile No. 2 has a positive bending moment at the junction between the pile top and the anti-sinking plate of 18.19 kN·m, the bottom of pile No. 2 has a positive bending moment of 0.185 kN·m. The bending moments of the two piles at a depth of 2.8 m are 0. The positive and negative signs of the bending moments at the pile tops are the same as those in the horizontal displacement diagram of the piles.

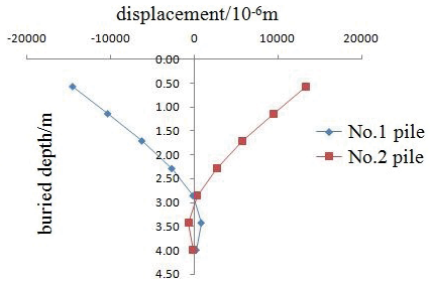

Fig. 11. Bending moments along the pile shafts in the y direction

The bending moments of the pile bodies in the z direction are shown in Fig. 12. The maximum negative moments of piles No. 1 and No. 2 are located at the tops of the piles and are 8644 N·m and 6406 N·m, respectively. The bending moments of pile No. 1 are greater than those of pile No. 2. The maximum positive bending moments of the two piles are located at a depth of 2.3 m and are 3260 N·m and 3302 N·m, respectively. The maximum positive bending moments of the two piles are relatively similar. The maximum bending moments are located at the tops of the piles, and the bending moments at the bottoms of the piles are approximately zero, which indicates that the confining effect of the soil at the bottoms of the piles is much less than the effect of the anti-sinking plate on the stabilization of the piles.

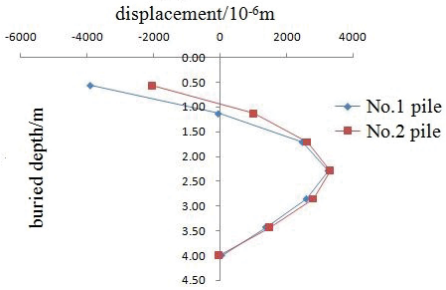

Fig. 12. Bending moments along the pile shafts in the z direction

CHARACTERISTIC ANALYSIS OF THE COMPOSITE FOUNDATION UNDER A VERTICAL LOAD AND BENDING MOMENT

SETTLEMENT ANALYSIS OF THE SEABED SOIL

The settlement characteristics of the seabed soil are shown in Fig. 13. In the figure, the normal surface is the section at the corner pile, and the settlement of the soil decreases radially with distance from the anti-sinking plate. The maximum soil settlement is 0.85 mm, and it occurs at the locations of piles No. 2 and No. 4. The vertical displacement of the seabed soil at the edge in the *x* axis direction is 0.027 mm, which indicates that the soil far from the mudmat-pile hybrid foundation is uplifted. The displacements at piles No. 2 and No. 4 pile are greater than those at piles No. 1 and No. 3, which indicates that the mudmat-pile hybrid foundation is inclined. As a result of the action of the angular pile, the soil settlement around the piles is significantly less than that far from the piles at the same depth. The effect of the angular piles decreases gradually with increasing distance from the piles, and the difference in the soil settlement caused by the pile essentially disappears at a depth of approximately 8 m. The results show that the presence of corner piles significantly reduces the settlement of the seabed soil body.

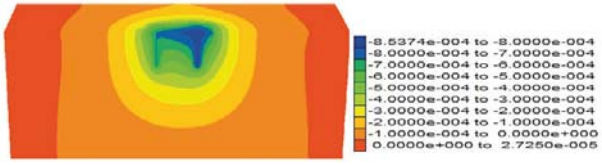

Fig. 13. Settlement of the seabed soil (unit: m)

ANALYSIS OF THE BENDING MOMENTS OF THE ANTI-SINKING PLATE

The bending moment of the anti-sinking plate due to the combined action of the vertical load and bending moment is shown in Fig. 14. Although the structure and the applied load are symmetrical, the bending moment diagram of the anti-sinking plate is not symmetric, and the bending moment distribution is complex.

As shown in Fig. 14(a), the maximum negative bending moment of the anti-sinking plate in the x direction is 21.282 kN·m, and it is located at the junction between pile No. 3 and the anti-sinking plate. The maximum positive bending moment is 6.75 kN·m and occurs in the middle of the long side of the anti-sinking plate. The area of the maximum positive bending moment is small and has little influence, whereas the area of the second highest positive bending moment is large and is located in the middle of the anti-sinking plate. The bending moments at the junctions between the four angle piles and the anti-sinking plate are between 15 kN·m and 21.282 kN·m, which are significantly greater than those at the other locations; this indicates that damage to the anti-sinking plate will occur at the junctions between the anti-sinking plate and the piles. As shown in Fig. 14(b), the maximum negative bending moment of the anti-sinking plate in the y direction is 14.444 kN·m, and it occurs at the connections between piles No. 3 and No. 4 and the anti-sinking plate. The maximum positive bending moment is 5.23 kN·m and is located along the long side of the anti-sinking plate. The bending moments of the anti-sinking plate are concentrated between 2 kN·m and 6 kN·m; only small areas of the edges and the junction between the corner piles and the anti-sinking plate are outside this range. The bending moments at the junctions between the corner piles and the anti-sinking plate are significantly greater than those at other locations, which indicates that damage to the anti-sinking plate can easily occur at the junction between the anti-sinking plate and the corner piles, which is the same as in the x direction bending moment diagram.

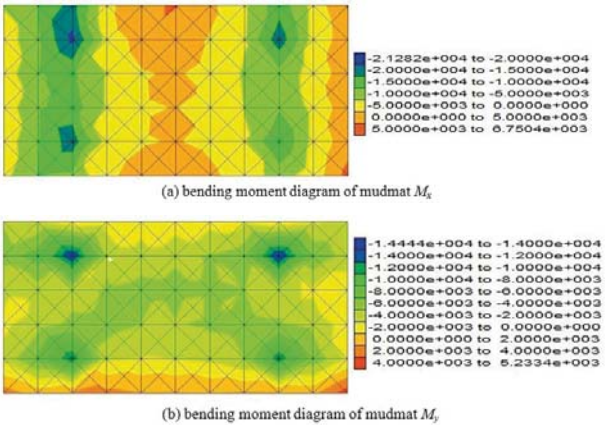

Fig. 14. Bending moments of the mudmat (unit: N·m)

ANALYSIS OF DISPLACEMENTS ALONG THE PILE SHAFTS

The horizontal displacements of piles No. 1 and No. 2 are shown in Fig. 15. Due to the combined action of the vertical load and bending moment, piles No. 1 and No. 2 move in the negative direction along the x axis at the bottom and forward along the x axis at the top. The top of pile No. 1 moves 5.143×10^{-6} m in the positive direction along the x axis, and the bottom moves 58.77×10^{-6} m in the negative direction. The top of pile No. 2 pile moves 3.97×10^{-6} m in the positive direction, and the bottom moves 16.88×10^{-6} m in the negative direction. The horizontal displacement lines of both piles are smooth curves, which indicates that the pile bodies are buckling. Piles No. 1 and No. 2 move in the same direction horizontally and tilt toward the x axis. The difference in displacement between the top and bottom of pile No. 1 is 63.91×10^{-6} m, and that of No. 2 pile is 20.85×10^{-6} m. The inclination angle of pile No. 1 is greater than that of pile No. 2.

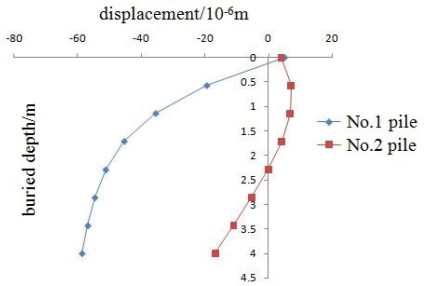

Fig. 15. Horizontal displacements along the pile shafts

The vertical displacements of pile No. 1 and No. 2 are shown in Fig. 16. The pile foundations move downward as a whole under the combined action of the vertical load and bending moment. The vertical displacements of the two piles form straight lines; the vertical displacement at the top of pile No. 1 is 0.7×10^{-3} m, and that at the top of pile No. 2 is 0.85×10^{-3} m. The displacements of the two pile tops are different, which indicates that the composite foundation is inclined.

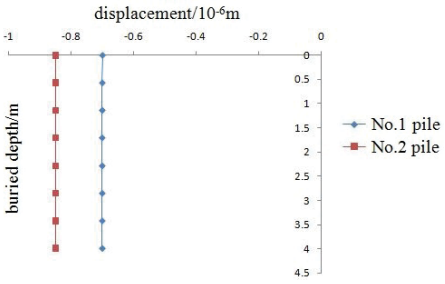

Fig. 16. Vertical displacements along the pile shafts

ANALYSIS OF THE BENDING MOMENTS ALONG THE PILE SHAFTS

The bending moments of the bodies of piles No. 1 and No. 2 are shown in Fig. 17 and Fig. 18. The bending moments of the pile bodies in the *x* direction are 0, so they are not analyzed. The bending moments of the pile bodies in the *y* direction are shown in Fig. 17. The maximum bending moments are located at the junctions between the pile tops and the anti-sinking plate, and the minimum bending moments are located at the bottoms of the piles, which indicates that pile damage can easily occur at the junctions between the pile tops and the anti-sinking plate. The bending moment at the top of pile No. 1 is 27.67 kN·m, and that at the bottom is 90.18 N·m. The bending moment at the top of pile No. 2 is 12.16 kN·m, and that at the bottom is 91.39 N·m. The bending moments of both piles decrease gradually from the top to the bottom and have opposite signs. The bending moments of pile No. 1 are greater than those of No. 2.

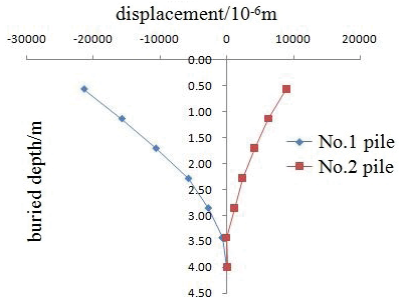

Fig. 17. Bending moments along the pile shafts in the y direction

The bending moment of the pile bodies in the *z* direction are shown in Fig. 18. The bending moment at the top of pile No. 1 is 11.26 kN·m, and that at the bottom of the pile is 0.72 N·m. The bending moment at the top of pile No. 2 is 6.67 kN·m, and that at the bottom of the pile is 42.79 N·m. The bending moment are largest at the tops of both piles, those at the bottoms are the smallest, and the signs are the same. The bending moment of pile No. 1 are greater than those of pile No. 2.

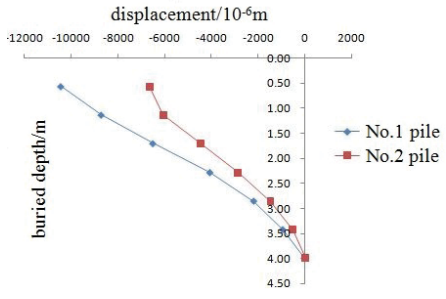

Fig. 18. Bending moments along the pile shafts in the z direction

CHARACTERISTIC ANALYSIS OF THE COMPOSITE FOUNDATION UNDER A HORIZONTAL LOAD AND BENDING MOMENT

SETTLEMENT ANALYSIS OF THE SEABED SOIL

The settlement characteristics of the seabed soil are shown in Fig. 19. In the figure, the normal surface is the section at the corner pile, and the amount of settlement decreases radially with distance from the composite foundation. The maximum settlement is 2.36 mm, and it occurs in the middle of the bottom of the anti-sinking plate. As a result of the action of the angular piles, the settlement of the soil around the piles is significantly less than that far from the pile at the same depth. With increasing distance from the angular piles, the effect of the piles decreases gradually, and the horizontal difference in the soil settlement caused by the piles essentially disappears at a depth of approximately 8 m. The angular piles influence the settlement of the seabed soil over a certain area, which is approximately twice the length of the piles.

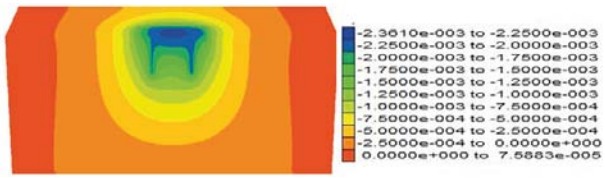

Fig. 19. Settlement of the seabed soil (unit: m)

ANALYSIS OF THE BENDING MOMENTS OF THE ANTI-SINKING PLATE

The bending moments of the anti-sinking plate due to the combined action of a horizontal load and bending moment are shown in Fig. 20. In general, the bending moments of the anti-sinking plate are not symmetrical, and the distribution pattern is not obvious.

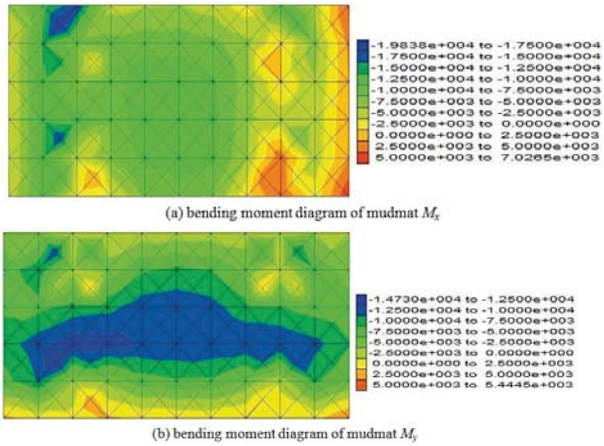

Fig. 20. Bending moments of the mudmat (unit: N·m)

As shown in Fig. 20(a), the maximum negative bending moment of the anti-sinking plate in the *x* direction is 19.838 kN·m, and it is located near piles No. 1 and No. 3. The maximum positive bending moment is 7.0265 kN·m, and it occurs at the corner of the anti-sinking plate along the *x* axis. The area of the maximum positive bending moment is small and has little influence. The bending moments of the anti-sinking plate are mainly between 10 kN·m and 12.5 kN·m, and they are located in the middle of the anti-sinking plate. The bending moments at the junctions between the piles and the anti-sinking plate are large. As shown in Fig. 20(b), the maximum negative bending moment of the anti-sinking plate in the *y* direction is 14.73 kN·m, and it is located between piles No. 1 and No. 3. The maximum positive bending moment is 5.4445 kN·m, and it occurs at the corner of the anti-sinking plate along the *x* axis. The area of the maximum positive bending moment is small, and its influence is not significant. The bending moments of the anti-sinking plate are mainly between 10 kN·m and 12.5 kN·m; they are located in the middle of the anti-sinking plate and are distributed in long strips in the *x* direction.

ANALYSIS OF DISPLACEMENTS ALONG THE PILE SHAFTS

The horizontal displacements along piles No. 1 and No. 2 are shown in Fig. 21. Due to the combined effects of a vertical load and horizontal load, pile No. 1 moves in the negative direction along the *x* axis, and pile No. 2 moves forward along the *x* axis. The top of pile No. 1 moves 4.139×10^{-6} m in the positive direction along the *x* axis, and the bottom moves 171.5×10^{-6} m in the negative direction. The top of pile No. 2 moves 0.2374×10^{-6} m in the negative direction, and the bottom moves 120×10^{-6} m in the positive direction. The horizontal displacements of piles No. 1 and No. 2 form smooth curves, which indicates that the pile bodies are buckling. Piles No. 1 and No. 2 move backward horizontally, the body of pile No. 1 pile leans in the negative direction along the *x* axis, and the body of pile No. 2 leans forward along the *x* axis. The difference in displacement between the top and bottom of pile No. 1 is 175.639×10^{-6} m, and that between the top and bottom of pile No. 2 is 120.24×10^{-6} m. The inclination angle of pile No. 1 is greater than that of pile No. 2.

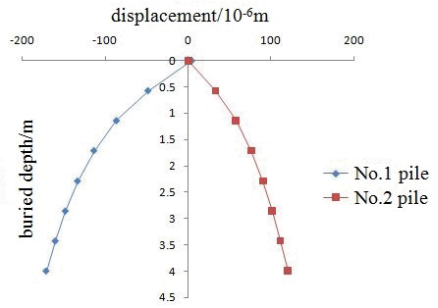

Fig. 21. Horizontal displacements along the pile shafts

The vertical displacements of piles No. 1 and No. 2 are shown in Fig. 22. The pile foundations move downward as a whole under the combined effects of the vertical load and horizontal load. The vertical displacement at the top of pile No. 1 is 2.037×10^{-3} m, and that at the top of pile No. 2 is 2.112×10^{-3} m. The vertical displacements at the tops of the two piles are different, which indicates that the composite foundation is inclined. The vertical displacements at the bottoms of the two piles are 2.032×10^{-3} m and 2.107×10^{-3} m, respectively. The vertical displacements of the pile bodies decrease, which indicates that the pile body is inclined; this is consistent with the results of the horizontal displacement analysis. The vertical displacements of the two piles form inclined nearly linear curves, which is mainly because the soil under the pile imparts a stress at the bottom of the pile, so the pile body experiences axial compression.

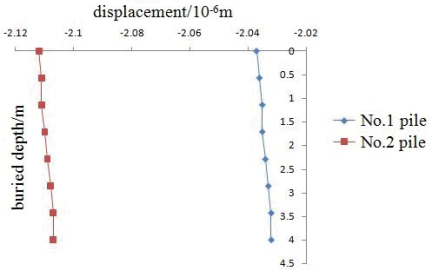

Fig. 22. Vertical displacements along the pile shafts

ANALYSIS OF THE BENDING MOMENTS ALONG THE PILE SHAFTS

The bending moments on the bodies of piles No. 1 and No. 2 are shown in Fig. 23 and Fig. 24. The bending moments of the pile bodies in the *x* direction are 0, so they are not analyzed.

The bending moments of the pile bodies in the *y* direction are shown in Fig. 23. The maximum bending moment of pile No. 1 is 49.11 kN·m, and it is located at the junction between the pile top and the anti-sinking plate. The minimum bending moment of pile No. 1 is 25.31 N·m, and it occurs at the bottom of the pile. The maximum bending moment of pile No. 2 pile is 28.49 kN·m, and it is located at the junction between the top of the pile and the anti-sinking plate. The minimum bending moment of pile No. 2 is 36.72 N·m, and it occurs at the bottom of the pile. The bending moments of pile No. 1 are greater than those of No. 2 pile body. The positive and negative signs of the bending moments at the bottom of the pile are the same as those shown in the horizontal displacement diagram of the piles; the results are the same as those of the horizontal displacement.

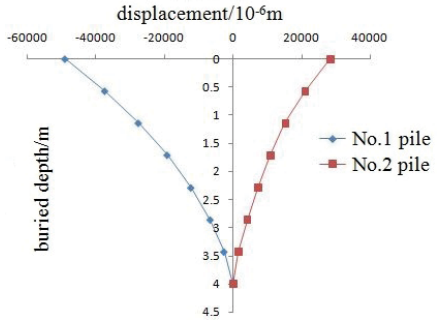

Fig. 23. Bending moments along the pile shafts in the y direction

Fig. 24 shows the bending moment of pile body in the *z* direction. The maximum bending moment of pile No. 1 is 26.54 kN·m, and it is located at the junction between the pile top and the anti-sinking plate. The minimum bending moment of pile No. 1 is 13.91 N·m, and it occurs at the bottom of the pile. The maximum bending moment of pile No. 2 is 22 kN·m, and it is located at the junction between the top of the pile and the anti-sinking plate. The minimum bending moment of pile No. 2 is 30.66 N·m, and it occurs at the bottom of the pile. The bending moments of pile No. 1 are greater than those of No. 2. Both piles have positive and negative bending moments in the vertical direction, and the positive bending moments are located in the lower half of the pile. The point of 0 bending moment on pile No. 1 is located at a depth of 1.7 m, and that on pile No. 2 is located at a depth of 1.5 m.

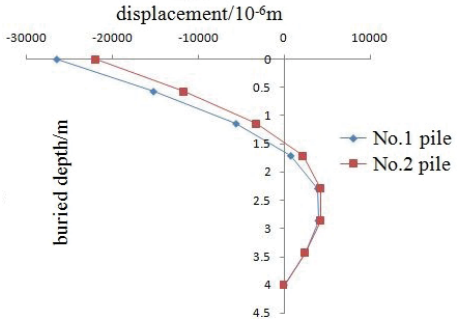

Fig. 24. Bending moments along the pile shafts in the z direction

CONCLUSION

A numerical model of a subsea mudmat-pile hybrid foundation is developed using the numerical simulation software FLAC3D, and the force and deformation characteristics of the model under different load combinations, including a vertical load and horizontal load, a vertical load and bending moment, and a horizontal load and bending moment, were analyzed. The main conclusions are as follows:

1. Due to the effect of the combined load, the seabed soil near the mudmat-pile hybrid foundation experiences settlement, whereas the soil far from the foundation is slightly uplifted. The presence of the pile foundation affects the settlement of the seabed soil, and the range of influence is approximately 2 times the length of the pile body.
2. Due to the effect of the combined load, the bending moment distribution of the anti-sinking plate is complex, and there are patterns under a vertical load and horizontal load but no clear patters under the other load combinations. The maximum bending moments of the anti-sinking plate occur at the junctions between the anti-sinking plate and the piles, which indicates that damage can occur easily in these locations.
3. Horizontal displacements along the pile shaft are produced by the combined loads. The horizontal displacement directions of piles No. 1 and No. 2 are opposite under a vertical load and horizontal load and under a horizontal load and bending moment load. The horizontal displacement directions of piles No. 1 and No. 2 under a vertical load and bending moment are the same. The pile bodies are inclined to varying degrees, and the tilt angle of pile No. 1 is greater than that of pile No. 2. The inclination directions of piles No. 1 and No. 2 are opposite under a vertical load and horizontal load and under a horizontal load and bending moment, whereas they are the same under a vertical load and bending moment.
4. The analysis of the bending moments along the pile shafts shows that the maximum bending moments occur at the junctions between the anti-sinking plate and the pile tops, which indicates that under a combined load, the piles are most vulnerable to damage at the junctions between the pile tops and the anti-sinking plate. Under a vertical load and horizontal load and a horizontal load and bending moment load, the pile bodies have points with a zero-bending moment.

ACKNOWLEDGMENTS

This study was financially supported by the National Natural Science Foundation of China (nos. 41372288).

BIBLIOGRAPHY

1. Bransby, M.F., Brown, M.J., Knappett, J.A.: Vertical capacity of grillage foundations in sand. *Revue Canadienne De Géotechnique*, 2011, 48(8), Pp. 1246-1265.

2. Brown, M.J., Bransby, M.F., Knappett, J.A.: The vertical capacity of grillage foundations. *Géotechnique,* 2012, 62(3), Pp. 201-211.

3. Chen, G.S., Liu, R.: Upper bound solutions of horizontal bearing capacity of skirted mudmat in sand. *Journal of Tianjin University (Natural science and Engineering Technology Edition)*, 2018, 53(3), Pp. 264-270.

4. Guan, W.W., Chen, L.: International vision of marine renewable energy management. *Modern Economic Information*, 1, Pp. 20-22.

5. He, Q., Wang, P.: Current Situation and prospect of deep-sea energy development. *Ocean Development and Management*, 2017, 34(12), Pp. 66-71.

6. Liu, B., Han, Y.H.: FLAC principles, examples and application guides. *Communications Press, Beijing*, 2005, pp. 67-68.

7. Lian, J.J., He, W., Wu, M.D.: Experimental study of bearing characteristic of bucket foundation of offshore wind turbine with bulkheads. *Rock and Soil Mechanics*, 2016, 37(10), Pp. 1-8.

8. Liu, R., Chen, G.S.: Upper bound solutions of vertical bearing capacity of skirted mudmat in sand. *The Ocean Engineering*, 2015, 34(4), Pp. 45-52.

9. Liu, R., Liu, M.M., Yang, S.G.: Bearing capacity of different shape mudmat foundations for subsea production system on undrained clays. *Acta Oceanologica Sinica*, 2016, 38(3), Pp. 131-144.

10. Liu, Y.M., Xu, D.P.: FLAC/FLAC3D foundation and engineering examples. *Water Conservancy and Hydropower Press, Beijing* 2008, Pp. 172-173.

11. Tan, Y., Liu, M.: Structure analysis of mudmat foundation for subsea production system. *Ship & Ocean Engineering*, 2012, 41(4), Pp. 133-135,141.

12. Xu, M.: Study of structural improvement of Mudmat in deep sea subsea system. *Master's thesis, Tianjin University, Tianjin, China*. 2015.

13. Xu, M., Yang, S.G., Wang, H.: Study of structural improvement of mudmat in the subsea system. *Marine Science Bulletin*, 2016, 35(4), Pp. 436-442.

14. Yun, G.J., Alasdair, M., John, O.: Undrained capacity of surface footings subjected to combined V-H-T loading. *Proceedings in the Nineteenth International Offshore and Polar Engineering Conference. Osaka*. 2009, Pp. 9-14.

15. Zhou, L., Liu, R., Guo, S.Z.: A dynamic simulation method for continuous spud can penetration. Journal of Earthquake Engineering, 2015, 37(2), Pp. 460-466.

16. Zhao, W.G., Liu, Y.T., Wang, W.S.: Current situation and development of marine renewable energy power generation. Smart Grid, 2015, 3(6), Pp. 493-499.

17. Ku Mohd Razali, K.H.N.S., Kasim, S., Hassan, R., Mahdin, H., Ramli, A.A., Md Fudzee, M.F., Salamat, M.A.: Lensalyza Photography Studio Reservation System. *Acta Electronica Malaysia*, 2018, 2(2), Pp. 06-09.

18. Li, B.Q., Li, Z.: Design of Automatic Monitoring System for Transfusion. *Acta Electronica Malaysia*, 2018, 2(1), Pp. 07-10.

19. Luo, X.: Research on Anti-Overturning Performance of Multi-Span Curved Girder Bridge with Small Radius. *Acta Mechanica Malaysia*, 2017, 1(1), Pp. 11-15.

20. Luo, X.: Study on PC Continuous Girder mechanical properties Based on Tendon Tensioning Pattern. *Acta Mechanica Malaysia*, 2017, 1(1), Pp. 16-20.

21. De'nan, F., Hasan, H., Mahzuz, M.: Behaviour of the beam to column connection for tapered steel section with perforation. *Engineering Heritage Journal*, 2017, 1(1), Pp. 41-44.

22. Kumar, R.: Comparison of Instruction Scheduling And Register Allocation For Mips And Hpl -Pd Architecture For Exploitation Of Instruction Level Parallelism. *Engineering Heritage Journal*, 2018, 2(2), Pp. 04-08.

CONTACT WITH THE AUTHORS

Desen Kong, Ph.D.
e-mail: skd992012@sdust.edu.cn

College of Civil Engineering and Architecture
Shandong University of Science and Technology
Qingdao Shandong
266590
China